Hindawi
Journal of Advanced Transportation
Volume 2019, Article ID 9540386, 15 pages
https://doi.org/10.1155/2019/9540386

*Research Article*

# Generating a Spatiotemporal Dynamic Map for Traffic Analysis Using Macroscopic Fundamental Diagram

**Yudi Li,[1] Lei Zhu,[2] Jian Sun ,[1] and Ye Tian [1]**

[1]*Key Laboratory of Road and Traffic Engineering in the Ministry of Education, Tongji University, Shanghai, 201804, China*
[2]*Department of Civil and Architectural Engineering and Mechanics, University of Arizona, Tucson, AZ, 85721, USA*

Correspondence should be addressed to Ye Tian; tianye@tongji.edu.cn

Received 18 April 2019; Revised 6 June 2019; Accepted 8 July 2019; Published 31 July 2019

Academic Editor: Rakesh Mishra



Transportation simulation and analysis projects that utilize maps with inappropriate fidelity levels carry a significant risk of having poor runtime or poor prediction performance. To address this, researchers use map abstraction method to abstract out a simplified map with fewer links and nodes based on the original full detailed map. Traditional static abstraction methods produce analysis maps with a single fidelity across the entire planning horizon, which cannot reflect the dynamic changes of daily traffic. This paper proposes a spatiotemporal dynamic map abstraction approach that adopts a time series clustering method to segment the analysis time horizon adaptively based on a Macroscopic Fundamental Diagram (MFD) curve, which describes network-wide dynamic traffic states. Time periods with similar macro-performance are grouped into one subinterval. A map with a dedicated fidelity is produced for each subinterval. Furthermore, a simulation is run on multiple abstracted maps with different fidelities in a sequence according to their temporal order. A numerical experiment ascertains that the proposed approach has promising results in both analysis accuracy and efficiency for resource-constrained modeling agents.

## 1. Introduction

Fidelity in traffic analysis refers to either simulation fidelity or network fidelity. The simulation fidelity is embodied in simulation models, such as macro-, meso-, and microscopic simulations. Network fidelity can be interpreted as the degree of detailed expression of a road network, which includes both map topological fidelity and link representation fidelity. The efficiency and accuracy of traffic analysis hinge on the topological fidelity of the network. A traffic network is essentially a spatially simplified and temporally discretized representation of a transportation system. The network topology fidelity level is often chosen at the modeling agents' discretion, based on the trade-off between runtime efficiency and prediction power.

The impact of the topological fidelity on efficiency and accuracy is indicated in Figure 1. Technically speaking, the impact of network topological fidelity on analysis accuracy is not simply linear. A map with excessively low fidelity that removes massive amounts of links and nodes can cause additional congestion. The increased traffic flow on the remaining links introduces additional simulation and assignment computational work load, therefore reducing efficiency. As for accuracy, a high-fidelity map with more links and nodes is able to guarantee analysis accuracy. However, the noncritical links in high-fidelity maps have no significant marginal effect on accuracy improvement and can be detrimental instead.

Although existing event-based mesoscopic traffic simulators are able to achieve a faster-than-real-time simulation performance in simulating city-scale networks [1, 2], the runtime may still fail if congestion builds up, or if it involves multiple rounds of simulations (as opposed to one-shot simulations in analysis tools such as Simulation-Based Dynamic Traffic Assignment (SBDTA) [3–5]). Further efficiency improvements of traffic analysis and simulation are in urgent demand and constructing a traffic analysis map with proper fidelity can help to improve analysis efficiency. This traffic map abstraction technique was developed to obtain these abstracted analysis maps that can produce flow patterns

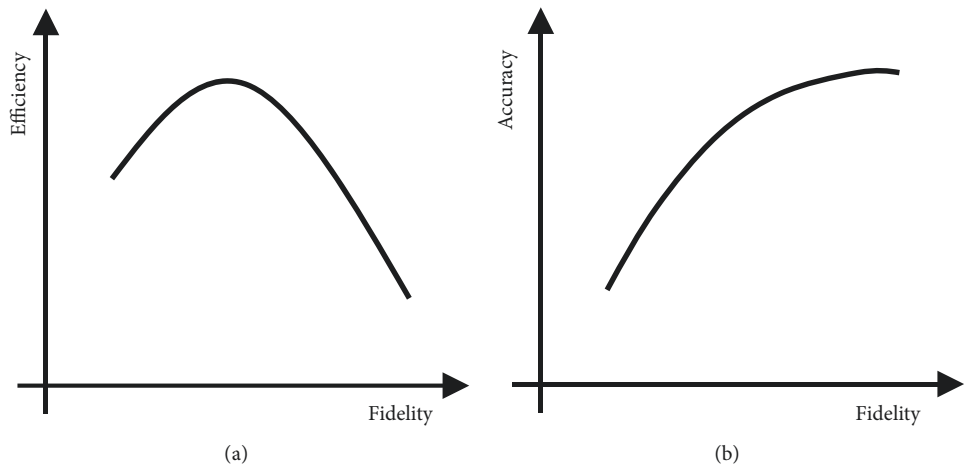


Figure 1: The impact of topological fidelity on the efficiency and accuracy of traffic analysis.

consistent with real traffic conditions and reduce computational burden under constrained computing resources.

The idea of aggregation has long been used in traditional map abstraction. A typical aggregation approach uses elements extraction [6]. Haghani and Daskin [7] used equilibrium link flow as the criteria to extract links and nodes that are identified as insignificant and formed an aggregate network. However, as shown in [8], traffic assignment procedures executed in such networks for multiple periods are computationally intractable.

In relevant map generalization and cartography studies, the concept of map abstraction is more about generating a legible and scale reduced map. For this, methods of network facility selection and deletion have been widely discussed [9]. Intelligent techniques, like the genetic algorithm [10] and concepts considering traffic characteristics like the shortest path-based algorithm [11], were used to generate more reasonable and convincing cartographic maps. However, such map generalization approaches ignore the connectivity requirement of a traffic network, and the resulting map may not be applicable to traffic analysis.

In the field of traffic analysis and modeling, early studies divided the traffic network into several research zones and took these zones as analysis units to model the network. Smith [12] pointed out that analysis zone size has an effect on traffic assignment results. Zonal aggregation provided a new approach to map abstraction, and the zones aggregated for traffic analysis are called Traffic Analysis Zones (TAZs). Eash, Chon [13] once proposed sketch planning on a simplified highway network by converting the road network to a grid network, with the regional zones aggregated to sketch-planning zones. However, this method caused a serious inconsistency problem due to the different spatial structures of the sketch planning zones and the complete network. Taking the vehicle routing transition brought about by map abstraction into consideration, a bush-based sensitivity analysis method [14] and improved bush based methods used for network contraction [15] were put forward successively. A contracted network only includes limited subnetworks, origins, and destinations, with artificial links connecting each OD pair. The network contraction procedure is conducted on the basis of the bush-based equilibrium sensitivity calculation. The advantage of these approaches is that they consider subnetwork diversions in the traffic assignment procedure.

In response to the problems of disconnectivity and vehicle routing selection, the Connectivity Enhancement Algorithm [16] selectively adds correctly classified critical links to a low-fidelity map and performs an efficiency topological shortest path searching procedure. The topological shortest path searching algorithm only takes the topological nearest neighbor nodes into the calculation of a shortest path, greatly narrowing down the search area. In order to better present the traffic dynamics, the authors improved the methodology of the original CEA and the SBDTA model is introduced in the link selection procedure [17]. This resulted in a sophisticated selection mechanism using Dynamic User Equilibrium (DUE) condition link travel time as the link cost to identify critical links. Thus, a more reasonable traffic analysis map abstraction method was formed.

However, all these approaches are static, which means that temporal traffic dynamics caused by vehicle movement and time-varying traffic demand is omitted. Static methods, such as the ones used to filter out low-class links, may also introduce prediction problems. As shown in Figure 2, a dense network with a complex network structure contains multiclass roads, and there are three main types of network topologies: the dense network, the broad network, and the sparse network. The broad network has distinct road classes, with flows mainly carried by high-class roads, whereas the sparse network contains limited high-class roads/bridges that connect several zones and either high-class or low-class roads serving those zones. A single static abstraction method cannot be adopted for these types of network topologies considering the inherent differences between the dense, broad, and sparse networks, especially for dense networks. In dense networks (mostly seen in European cities), the flow volume discrepancy between various classes of roads is not significant within low-class roads that also serve as critical

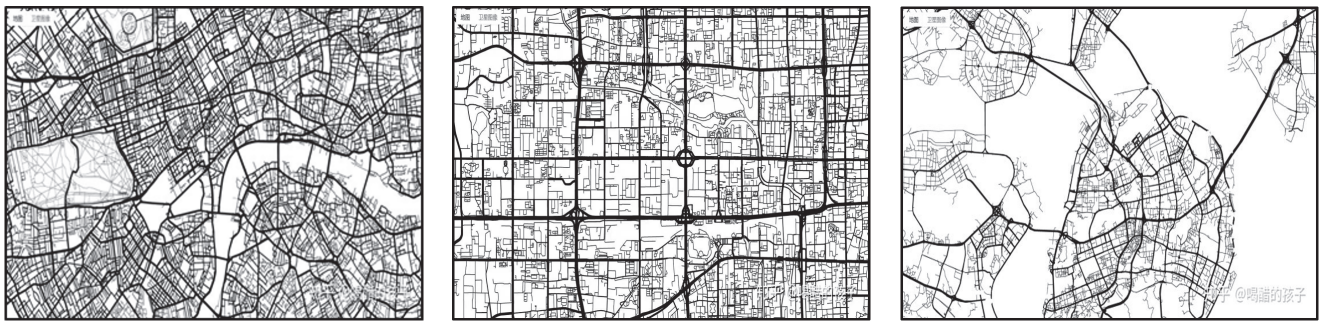

(a) Dense network (London, UK) (b) Broad network (Beijing, China) (c) Sparse network (Xiamen, China)

Figure 2: Different types of road network topology.

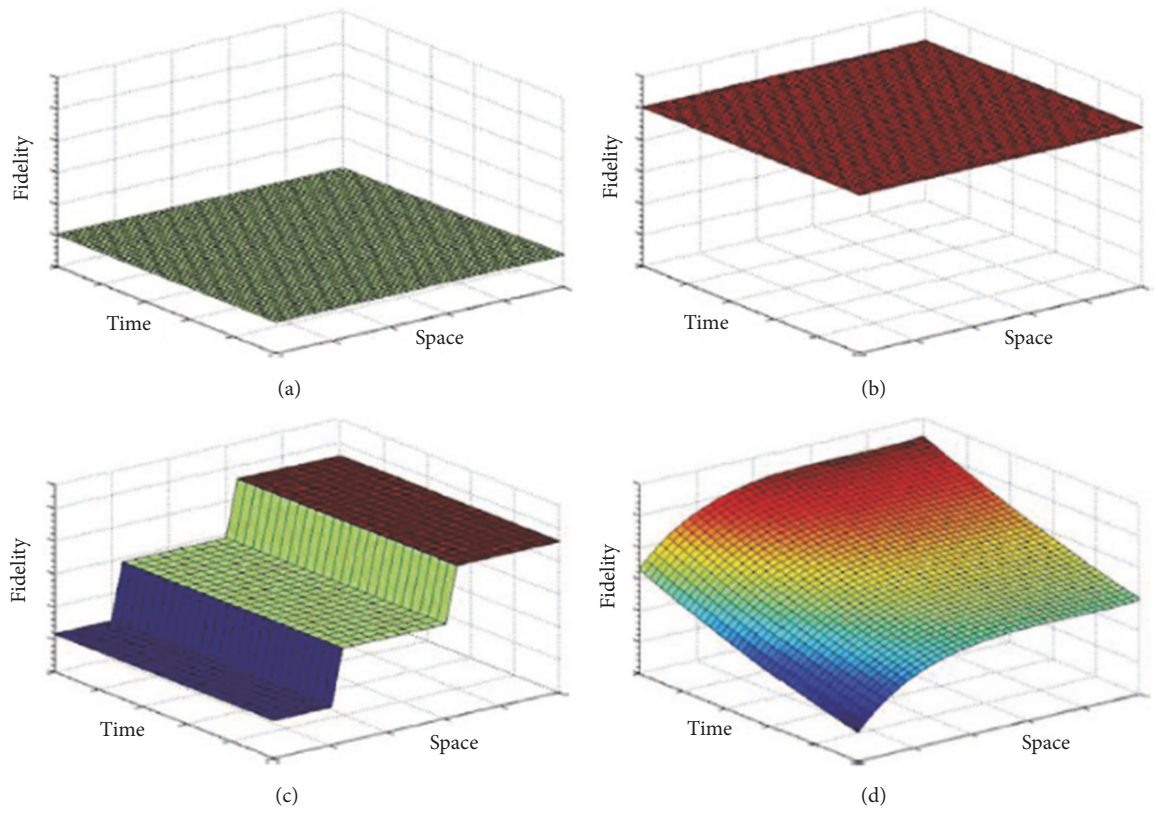


Figure 3: Conceptualization of simulations in spatial–temporal fidelity domains: (a) mesoscopic, (b) microscopic, (c) hybrid, and (d) adaptive [34].

links for certain OD pairs. One can thus imagine that static abstraction methods are not applicable for identifying critical links within these dense networks.

A hybrid simulation idea incorporating macro-, meso-, and micro-counterparts in one single map has been raised recently. The motivation of using hybrid simulations is simple and straightforward. A single analysis map with fixed fidelity, like Figures 3(a) and 3(b), may not be able to cope with the spatial fluctuations in a real road network. The integration of analysis maps with different fidelities is highly desirable for real world applications. Taking spatial heterogeneity into account, there exist hybrid fidelity simulation models, like AIMSUN and TransModeler [18], that apply maps with different fidelities to different regions. User defined physical boundaries are adopted to ensure network connectivity. As a result, the topological fidelity may or may not be identical in different regions. Combining different fidelity models enables detailed analysis of some interesting subareas as well as overall analysis of whole road network. This spatially integrated simulation map technique is helpful for spatially dependent fidelity adjustable network building. This is because they are inherently only adaptive in the spatial domain but not in the temporal domain, as shown in Figure 3(c). Such modeling approaches can be termed as semidynamic approaches.

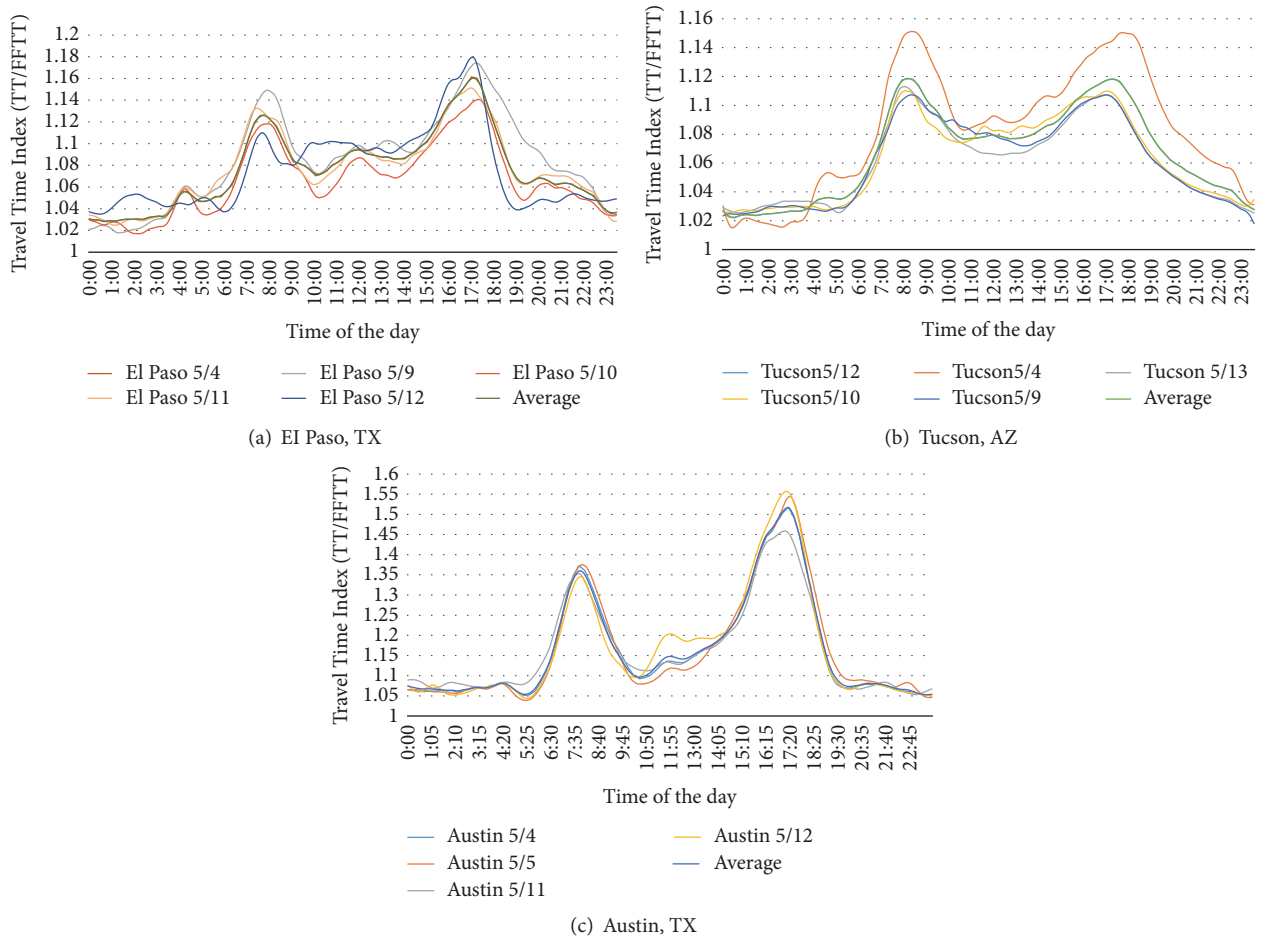


(a) EI Paso, TX

(b) Tucson, AZ

(c) Austin, TX

Figure 4: Temporal and network heterogeneity of traffic patterns.

However, the spatial-dependent methods solely care about the spatial heterogeneity of traffic patterns and omit the temporal variations of traffic within a day to some extent. Figure 4 shows the daily (5 days a week) traffic patterns in three U.S. cities (EI Paso, TX, Tucson, AZ, and Austin, TX). As one can see, the traffic flow fluctuates within each day for each city. Peak hours and nonpeak hours coexist every single day. Therefore, time heterogeneity needs to be considered as well in the process of traffic map abstraction. Figure 3(d) presents an idea known as adaptive simulation that can spatiotemporally adjust map or modeling fidelity. Moreover, traffic distribution varies across different cities. Such variance calls for unique abstraction schemes for each city. Thus, the abstraction method should be time-dependent and network-dependent to create an adaptive map representation. The above network dynamic can be characterized using Macroscopic Fundamental Diagram (MFD).

A MFD is a type of fundamental diagram [19] that describes the overall traffic state of a road network in terms of network average flow, density, and speed [20], and it can reflect the entire road network's dynamic characteristics during the analysis period in an aggregate manner. By modeling large urban regions in an aggregated manner, Geroliminis and Daganzo [21] first raised the concept of MFD. In 2008, a field experiment in Yokohama (Japan) verified the existence of MFD based on traffic flow data collected by fixed sensors (loop detectors) and mobile sensors (floating car) [20, 22].

The proposal of MFD inspired many scholars to study its shape, properties, and applications, and design various MFD-based traffic management and control strategies. In the Yokohama experiment, Geroliminis and Daganzo [20] pointed out that in an urban neighborhood, there approximately exists a well-defined MFD that relates the accumulation of vehicles to its space-mean flow. A reproducible MFD also reveals a robust relationship between the neighborhood's internal production and its outflow. As such, Geroliminis and Sun [23] investigated the desirable properties of the network to ensure a well-defined MFD and also pointed out that due to hysteresis effects, freeway networks did not have well-defined MFDs. Based on the concept and properties of MFD, it can be used to improve urban accessibility and formulate traffic control strategies.

Because real-life large-scale traffic networks have multiple levels of roads, network heterogeneity may impact the shape of the MFD. Therefore, the idea of network partitioning

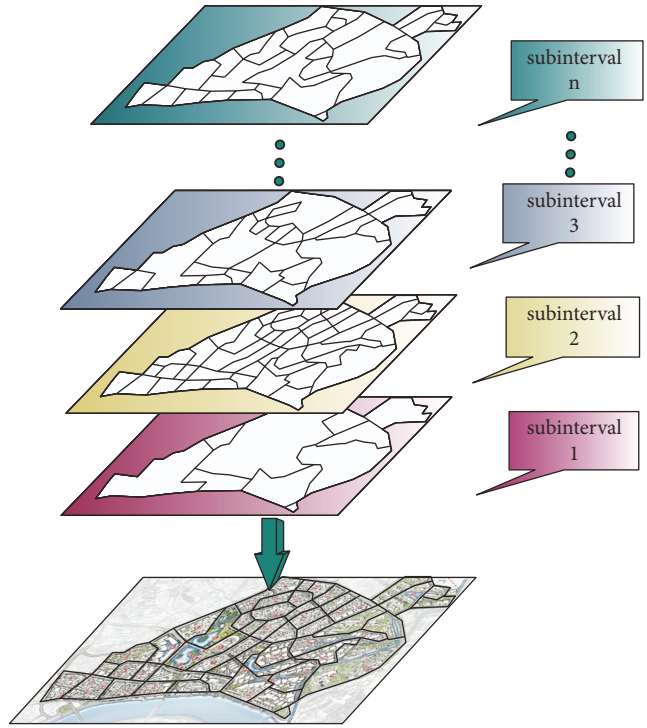


Figure 5: Full-dynamic map.

has been raised by some researchers [24, 25]. The network partition theory divides the network into several subnetworks, each with a well-defined MFD, which then enables traffic managers to formulate hierarchical traffic management strategies. In addition to online traffic control methods such as routing strategies [26] and area metering control [27], traffic demand management strategies like pricing policies and parking management can also be implemented on the subnetworks to evaluate their effectiveness [28, 29].

Considering the evidently temporal variability of traffic dynamics, there have also been studies that temporally clustered the planning time horizon based on MFD to help detect homogeneous time periods. Pascale, Mavroeidis [30] used a spectral clustering method to divide the morning peak hours (6:00-10:55 a.m.) into two separate clusters and detected the increasing and constant trends of the density averaged over the network. Thus, the MFD clustering method opened up a new path to explore the features of an entire traffic network in the temporal dimension. Because a MFD is a time-continuous curve, traditional distance-based clustering may result in ambiguous boundaries, i.e., jumping segmentation critical points.

As the concept of MFD is relatively new, to the best of the author's knowledge, existing applications of MFD are limited. In recent years, the practical application of MFDs has become a hot research area. Ampountolas, Zheng [31] applied a bimodal MFD to mixed traffic for congested single- and multiregion urban networks. Kim, Tak [32] combined the concept of agent, MFD, and the original cellular transmission model and proposed a network transmission model for large urban traffic. A MFD can also be used in link criticality evaluation, as Kim and Yeo [33] noted.

To overcome the shortcomings of the static and semi-dynamic (spatial dynamic) map abstraction approaches, we propose a full-dynamic, or adaptive (both temporal and spatial) map abstraction framework that can adjust the fidelity of a map with reference to both temporal and spatial traffic dynamics. Figure 5 illustrates the concept of a full-dynamic map. We intuitively refer to MFD to characterize the temporal dynamics of the transportation network. A time-series clustering method is adopted to segment the within-day MFD curve, and to further obtain sequential subintervals with nearly the same macro-network performance. Then, the Connectivity Enhancement Algorithm (CEA) is performed to generate an abstracted map for each subinterval with noncritical links removed. A traffic analysis tool (SDBTA in our case) can then be run on a network that is adaptive in the spatiotemporal domain.

The paper is organized as follows: Section 2 introduces the methodology of adaptive traffic analysis map abstraction. A case study on a real world network in a mesoscopic SBDTA simulation model is elaborated on in Section 3. Finally, Section 4 concludes the study.

## 2. Methodology

The purpose of the proposed spatiotemporal dynamic map abstraction method is to abstract a series of abstracted maps with varying fidelities to fit the traffic dynamics of different time periods.

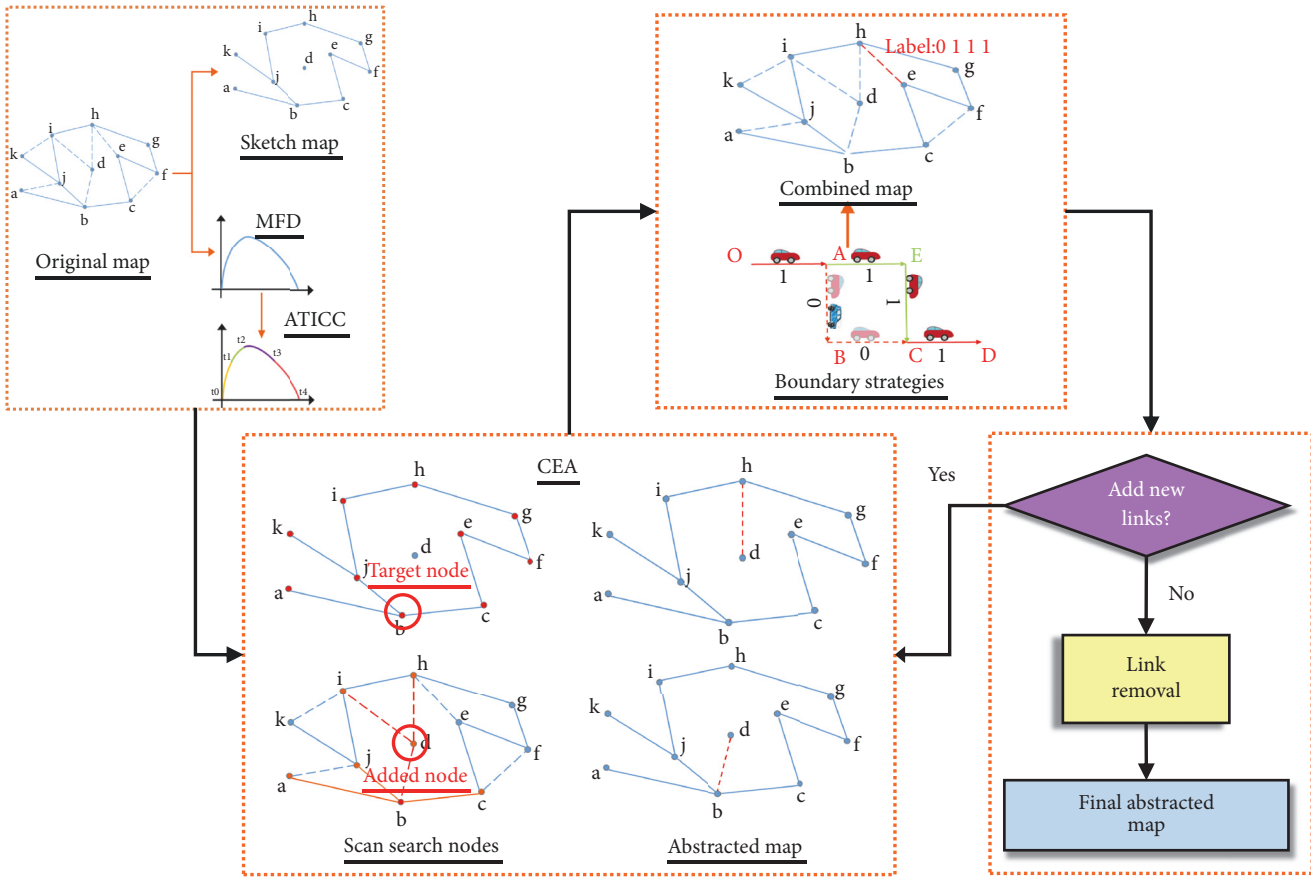


Figure 6: Workflow of the spatiotemporal dynamic map abstraction method.

*2.1. Overall Workflow of Spatiotemporal Dynamic Map Abstraction.* The overall workflow of the proposed spatiotemporal dynamic map abstraction method is presented in Figure 6.

The abstraction starts from a detailed original map, and the sketch map with only high-class roads retained is directly extracted from the original map. What needs to be guaranteed is that there must exist at least one generation link and one destination nodes in each TAZ. Thus, the vehicles entering can at least find one path out. The MFD chart can be plotted after calculating the network-wide average flow, density, and speed. According to the macro performance of the analysis traffic network, the MFD-based time series clustering method, Advanced Toeplitz Inverse Covariance-Based Clustering (ATICC) then clusters the MFD curve and segments the time horizon into multiple subintervals. For each subinterval $s$, the network expanding method, Connectivity Enhancement Algorithm (CEA), is executed. CEA identifies the critical links and expands them onto the sketch map.

Once a series of abstracted maps is obtained, they are integrated and applied to SBDTA. SBDTA provides a network-wide Dynamic User Equilibrium (DUE) flow pattern, which is adopted as the input to CEA to embody traffic dynamics. It is worth mentioning that three unique strategies are adopted herein to cope with the boundary issues caused by temporal segmentation between the sequentially abstracted maps. (1) Data preparation: all links in the abstracted maps are labeled with their status against the original map in the corresponding abstracted map (i.e., "1" means existence in the abstracted map while "0" means nonexistence in the abstracted map). The labeled abstracted map configuration serves as the input file of SBDTA. (2) Simulation: in order to ensure the simulation procedure executes without interruption, those vehicles traveling on the removed links, whose labels shift from "1" to "0", would stop moving until the label returns to "1". (3) Assignment: the "0" links are omitted when calculating the time-dependent shortest path (TDSP), and the impacted vehicles will make en-route changes. The reason for the adoption of these strategies is that the removed noncritical links generally have limited traffic flow and most of the affected vehicles would simply change their paths to avoid the deleted links. Only a few vehicles would be caught in the deleted links. The above strategies do not have a significant impact on the overall prediction performance, as will be shown later in this paper.

The iteration of CEA and SBDTA continuously adds critical links to the sketch map and will stop once the abstracted map reaches stability; i.e., the map cannot be expanded any more. With the expanded abstracted map generated, the postprocessing procedure is then performed to remove misclassified links with almost no traffic flow and to

deal with the dis-connectivity problem. After the completion of the postprocessing procedure, the final abstracted dynamic map can be exported.

The major steps of the proposed adaptive map abstraction method are outlined below.

*Step 1.* Prepare the original map and extract the sketch map, run SBDTA on the original map, and calculate the network average traffic flow, density, and speed.

*Step 2.* Run ATICC to cluster the MFD curve and get the planning horizon segmentation scheme.

*Step 3.* Run CEA on the sketch map for each subinterval to expand the map.

*Step 4.* Combine a series of sequential abstracted maps with different fidelities and label the links against the original map.

*Step 5.* Handle the boundary issues. Run SBDTA to get the DUE solution.

*Step 6.* Check whether new links can be added to the abstracted maps, and if there are none, stop criterion is satisfied. Otherwise, go back to Step 3.

*Step 7.* Postprocessing procedure is performed, and selectively remove the noncritical links and guarantee network connectivity.

The following segment introduces the MFD-based time series cluster (Step 2) and CEA (Step 3), which are the two major components within the abstraction procedure.

*2.2. The MFD-Based Time Series Clustering.* In consideration of the temporal continuity of the MFD curve, it is reasonable to consider the traffic flow, density, and speed as time series and to encourage adjacent sequences to be clustered together. The clustering algorithm adopted here is Advanced Toeplitz Inverse Covariance-Based Clustering (ATICC).

The definitions of space-mean traffic flow, density, and speed are

$$\overline{q} = \frac{\sum_{a=1}^{n} q_a}{n} \tag{1}$$

$$\overline{k} = \frac{\sum_{a=1}^{n} l_a lane_a k_a}{\sum_{a=1}^{n} l_a lane_a} \tag{2}$$

$$\overline{v} = \frac{\overline{q}}{\overline{k}} \tag{3}$$

where $\overline{q}$, $\overline{k}$, $\overline{v}$ represent the network average traffic flow, densit,y and speed, $q_a$, $k_a$ are the flow and density of link $a$, and $l_a$, $lane_a$ denote link $a$'s length and number of lanes.

ATICC was developed based on the fundamental multivariate time series data clustering approach, Toeplitz Inverse Covariance-Based Clustering (TICC) [35]. Different from conventional distance-based metric clustering methods, TICC is a model-based method. Therefore, instead of describing the similarities of time series simply by their distance, model-based methods can better measure the correlations between the series and shows good robustness and stability in multivariate time series data clustering.

Suppose that $X_{orig}$ is a $n$-dimensional time sequential data with a duration $T$, and $x_l$ ($x_l \in X_{orig}$) is the $l$-th multivariate vector. In order to guarantee the continuity of adjacent time series data, a short subsequence of size $w$ ($w \ll T$) is treated as a whole and recorded as $X$. Subsequence $X_t$ consists of vector $x_{t-w-1}$ to vector$x_t$ and is a $nw$-dimensional vector. The subsequences are expected to be clustered into $K$ clusters, with each cluster defined as a Markov Random Field (MRF), showing how the network performance at time$t$ will affect the successive performance at time $t + 1$. A sparse Gaussian inverse covariance matrix $\Theta$ [36] is defined as an adjacency matrix of each cluster to show the dependencies between the subsequences from each dimension at each time, and $\Theta = \{\Theta_1, \ldots, \Theta_K\}$. $\Theta_i$ is a $nw \times nw$ matrix and can be expressed in the following form:

$$\Theta_i = \begin{bmatrix} A^{(0)} & \left(A^{(1)}\right)^T & \left(A^{(2)}\right)^T & \cdots & \cdots & \left(A^{(w-1)}\right)^T \\ A^{(1)} & A^{(0)} & \left(A^{(1)}\right)^T & \ddots & & \vdots \\ A^{(2)} & A^{(1)} & \ddots & \ddots & \ddots & \vdots \\ \vdots & \ddots & \ddots & \ddots & \left(A^{(1)}\right)^T & \left(A^{(2)}\right)^T \\ \vdots & & \ddots & A^{(1)} & A^{(0)} & \left(A^{(1)}\right)^T \\ A^{(w-1)} & \cdots & \cdots & A^{(2)} & A^{(1)} & A^{(0)} \end{bmatrix}, \tag{4}$$

where $A^{(t)} \in \mathbb{R}^{n*n}$ denotes the correlation of data in each dimension at time t. Here, $A^{(0)}$ subblock represents the intratime partial correlations, so $A^{(0)}_{jk}$ refers to the relationship between concurrent values of n-dimensional time series $j$ and $k$ at time $t_0$. $A^{(1)}$ shows the correlation of time series at time $t_0 + 1$ [35].

Thus, $\Theta_i$ represents the correlation among the $n$-dimensional data of cluster $i$ in a time window of $w$, and it has a block Toeplitz structure, which can be learned by solving a constrained inverse covariance estimation problem called *Toeplitz graphical lasso*.

The overall TICC problem can be expressed as follows:

$$\operatorname{argmin}_{\mathrm{P},\Theta\in\Gamma} \sum_{i=1}^{K} \left[ \left\| \lambda \circ \Theta_i \right\|_1 + \sum_{X_t \in P_i} \left( -\ell\ell\left(X_t, \Theta_i\right) + \beta \mathbb{I}\left\{X_{t-1} \notin P_i\right\}\right) \right] \tag{5}$$

where $\Gamma$ is the set of block Toeplitz matrices, $P$ is the set of point assignment, and each $P_i$ contains the time series assigned to cluster $i$. $\|\lambda \circ \Theta_i\|_1$ is a $l1$-norm penalty to incentivize a sparse inverse covariance and to prevent

overfitting, $\lambda$ is a parameter that determines the MRFs' sparsity, $\ell\ell(X_t, \Theta_i)$ is the log likelihood that $X_t$ belongs to cluster $i$, $\mathbb{I}\{X_{t-1} \notin P_i\}$ is a function used to determine whether the adjacent subsequence $X_{t-1}$ comes from the same cluster as $X_t$, and $\beta$ is a penalty parameter imposed to encourage temporal continuity. If the adjacent times are to be clustered into different cluster, a penalty of $\beta$ will be imposed. The larger $\beta$ is, the stronger the tendency of adjacent sequences to be clustered into one cluster. The problem has two unknown parameters, $\Theta$ and $P$, which means there are two subproblems needed to be solved. Each assignment scheme $P$ corresponds to a parameter set $\Theta$. By initializing the parameter $\Theta$ and $P$, the algorithm alternates to adjust the assignment scheme $P$ and further update the cluster parameter $\Theta$ until they get stabilized. The final converged solution is the optimal assignment scheme.

In adopting TICC to perform time horizon segmentation in the map abstraction experiment, the unique features of traffic flow data, i.e., the existence of morning and evening peak hours, should be taken into consideration. The original TICC needs to be modified, and we propose the updated clustering method, ATICC.

The MFD-based temporal clustering of traffic analysis networks is the focal point of ATICC. To facilitate the analysis of traffic pattern differences between peak and nonpeak hours, the tendency is to separate out peak hours. As such, another penalty parameter $\beta'$, which is less than or equal to $\beta$, is introduced and acts to increase the tendency to isolate both morning and evening peak hours. The overall optimization problem is rewritten in the following form:

$$\operatorname{argmin}_{P,\Theta\in\Gamma} \sum_{i=1}^{K} \left[ \|\lambda \circ \Theta_i\|_1 + \sum_{X_t} \left( -\ell\ell\left(X_t, \Theta_i\right) + \beta \mathbb{I}\left\{X_{t-1} \notin P_i\right\} + \beta' \mathbb{I}\left\{X'_{t-1} \notin P_i\right\} \right) \right] \quad (6)$$

where $\mathbb{I}\{X'_{t-1} \notin P_i\}$ is a function used to determine whether the adjacent subsequence $X'_{t-1}$ from peak hours comes from the same cluster as $X_t$.

A smaller $\beta'$ makes it more likely to separate out peak hours. In practice, $\lambda$ and $\beta$ can be user-defined, while $\beta'$ should be determined by corresponding traffic conditions. A reasonable time interval number $S$ is preset, and the final optimal segmentation scheme is used as the one that minimizes the sum of the standard deviation of traffic density in each subinterval. Here, the cluster number $K$ is not necessarily equal to time interval number $S$. Taking the temporal sequence "1,2,3,2,1" as an example, $K$ is equal to three, while there are five intervals, which means $S$ is generally greater than or equal to $K$. The value of $\beta'$ can be calculated by

$$\beta' = \arg\min \sum_{s=1}^{S} \left( \sqrt{\frac{\sum_{t=1}^{n} \left( k_t\left(\beta'\right) - \bar{k}\left(\beta'\right) \right)^2}{n-1}} \right) \quad (7)$$

where $k_t(\beta')$ is the network density at time $t$ and $\bar{k}(\beta')$ is the average density of subinterval $s$.

*2.3. Review of Connectivity Enhancement Algorithm (CEA).* The traffic analysis map of each subinterval needs to be abstracted separately based on the division plan of ATICC. The Connectivity Enhancement Algorithm (CEA) is an efficiency dynamic map abstraction method, which helps to catch critical links. It contains two main procedures: Topological Nearest Neighbors Search (TNNS) [37] and Shortest Path (SP) comparison.

TNNS is an efficiency node search algorithm, which considerably reduces the search scope. Each node of the sketch map acts as a search node for the first round of searching. Starting from one search node, it performs Breadth-First-Search (BFS) [38] for all directions on the original map to find the topological nearest neighbors (TNNs) of the chosen node. More specifically, TNNs are defined as the nearest nodes to the search node that belong to the sketch map or reach the edge of the original map.

The SP comparison procedure then computes the shortest path costs (DUE travel time) from each search node to its TNNs and compares the costs of the sketch map and original map, respectively. For the same OD pair, if the SP cost ratio between the original map and sketch map is less than or equal to a given constant (greater than one), the original map's shortest path and the corresponding nodes will be expanded to the sketch map. The nodes added after SP comparison continue as the search nodes and are passed to the next iteration. By taking DUE travel time as the link cost, this SP comparison procedure can accurately capture traffic dynamics.

By alternating TNNS and SP comparison procedures, the sketch map is expanded. CEA stops when all search nodes are visited, and no more links can be added. The ultimate expanded sketch map is then exported as an initial abstracted map.

## 3. Case Study

In order to demonstrate the feasibility and effectiveness of the proposed method, the spatiotemporal dynamic map abstraction approach is applied to a real transportation network–the Alexandria network. DynusT [39, 40] is adopted to perform traffic simulation and dynamic traffic assignment.

*3.1. Experiment Configuration.* The Alexandria network is a high-fidelity digital map with detailed road information, and was downloaded from Open Street Map [41]. There are 85 TAZs, 6,724 links, and 2,573 nodes in the entire analysis traffic road network, which contains various levels of roads. High-class roads like freeways are retained to form a size-concise and connected sketch map. The original map and the sketch map are shown in Figure 7.

The planning time horizon covers 24 hours (1,440 minutes), which is consistent with the OD demand matrix time range. The traffic demand amount file is derived from the US Census Bureau Public Use Microdata Sample. We derived the network MFD curve based on the dynamic traffic flow and density patterns obtained from the initial SBDTA run. Figure 8 shows how the network average flow and density fluctuate over time within the time horizon.

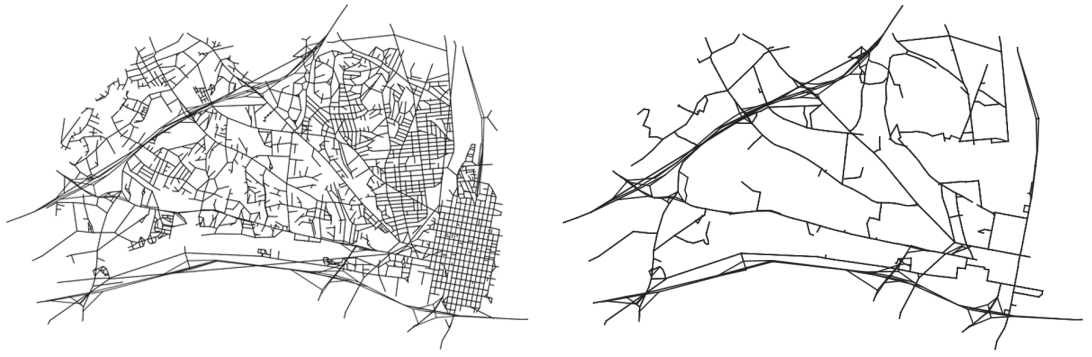

(a) (b)

Figure 7: Analysis traffic maps: (a) original map, (b) sketch map.

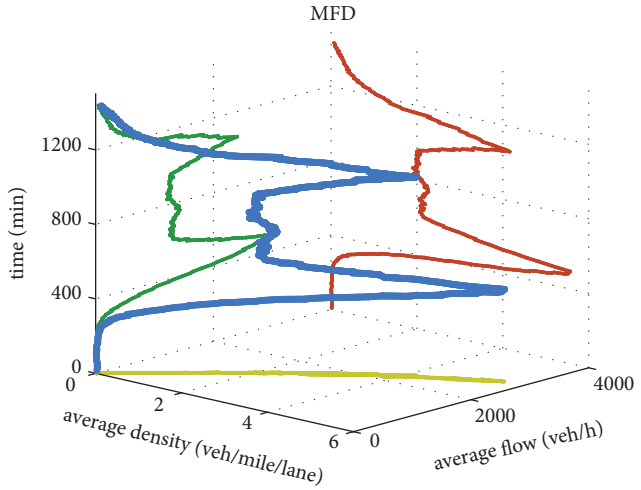


Figure 8: Network MFD (the projection in green is the time-dependent flow pattern, the projection in red is the time-dependent density pattern, and the projection in yellow is the relationship between flow and density).

*3.2. Numerical Results.* The planning horizon segmentation result of ATICC and the statistical information of each abstracted map is summarized and elaborated in the following parts.

*3.2.1. Segmentation of Planning Horizon.* ATICC is performed here to simultaneously cluster the MFD data points and further segment the planning time horizon. Based on the macro traffic performance presented by the MFD, it intends to segment the time horizon into six subintervals, i.e., the subinterval number $S = 6$. Given a reasonable penalty parameter value, $\beta$=300, the calibrated value $\beta'$ is 295 based on (7), and the duration of each subinterval is 255 min, 120 min, 225 min, 385 min, 180 min, and 280 min, respectively. We plot the ATICC clustering results in Figure 9 with different clusters marked in different colors.

To demonstrate the rationality of the clustering scheme, the traffic demand distribution of each analysis period is given in Figure 10. One can note that both peak hours and peak periods are successfully grouped into a single cluster and that the time ranges are $[375, 595]$ and $[980, 1160]$, respectively, for morning and evening peak periods. At the same time, the nonpeak hours and the trends of demand growth and decline are identified by the proposed ATICC clustering algorithm.

Compared with the nonsegmentation MFD, the main advantage of the time series data segmentation scenario is that the traffic behavior remains nearly identical over the network in the same cluster, with the standard deviations for each cluster at 0.016, 0.451, 1.110, 0.097, 0.550, and 0.436, respectively. To interpret the difference of network density between adjacent subintervals, Student's t test was adopted. The null hypothesis suggests that there exists no statistical significance in two sets of given observations. With a significance level of 0.05, the P-value is equal to 0.000 in each test between adjacent subintervals, which is less than 0.05. Therefore, we reject the null hypothesis.

*3.2.2. Map Abstraction.* Once the time horizon segmentation scheme is obtained, the CEA and SBDTA are iteratively executed for each subinterval, and 6 initial abstracted traffic analysis maps with different fidelities can be exported.

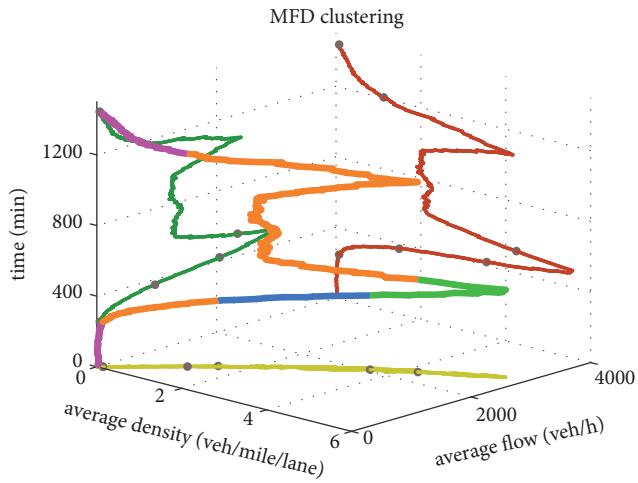


Figure 9: ATICC clustering result. Each color stands for one cluster with peak hours identified and captured.

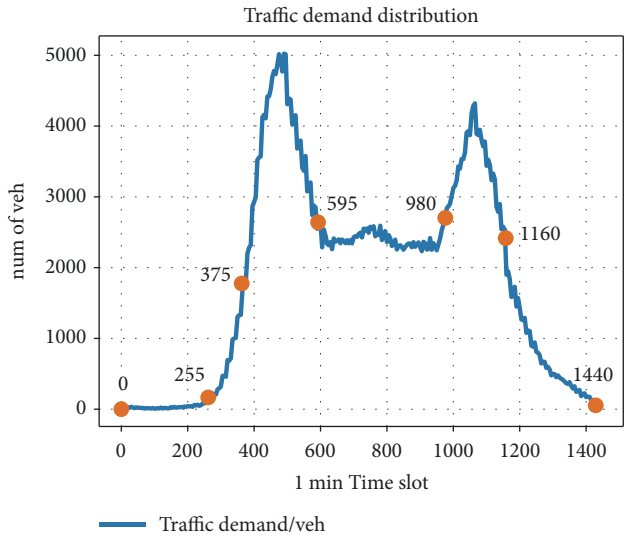


Figure 10: Subinterval traffic demand distribution.

Table 1 summarizes the statistics of the six abstracted maps and the original map. The link number is reduced by more than half, from the original 6,724 to less than 3,000, along with a similar reduction in node number. Meanwhile, one can tell that the abstracted maps for peak periods (sub_3 and sub_5) with higher average density contain more links and nodes compared to that for nonpeak periods.

Figure 11 shows the abstracted maps for each subinterval. The black thick lines denote the sketch map and the red thin lines represent the newly added links according to CEA. One can tell that those abstracted maps in the time periods with heavy traffic demand, such as "sub_3", "sub_5", allow more links and nodes. On the other hand, "sub_1" is almost the same as the sketch map with no additional links, as the traffic demand in the first subinterval (i.e., 0-255 min) is much lower compared to other subintervals. It is consistent with the observations in Table 1.

What is more, the spatial distribution can also be captured. The eastern area of the map is apparently denser and has more links added. Therefore, the fidelity of the analysis map is adjustable in both spatial and temporal dimension, which implies the realization of adaptive topological map representation.

*3.3. Results Validation and Analysis.* The final series of abstracted maps is fed into the SBDTA model. The performance statistics of SBDTA on the dynamic map and the original full static map with identical traffic demand are shown in Table 2. The average travel time and distance are used to evaluate the accuracy of the method, and the efficiency enhancement is expressed by the computational time. At the same time, the average travel times of the affected vehicles are utilized to access the impact of the boundary issues.

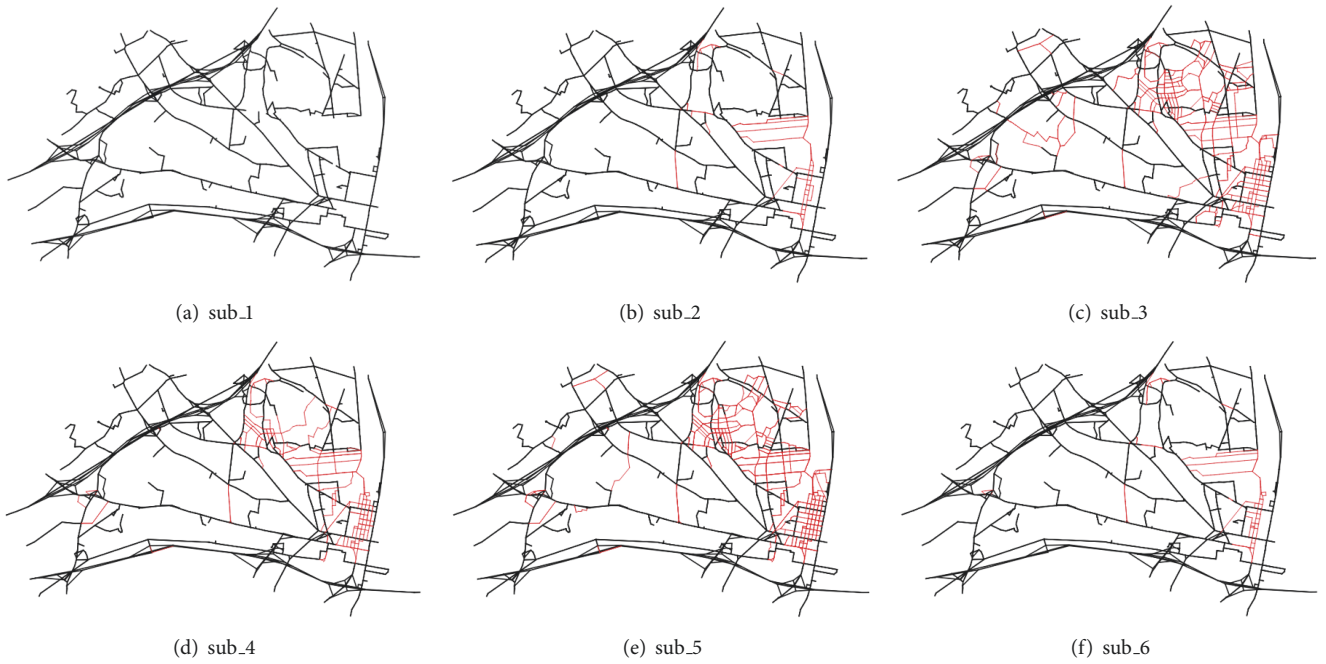

(a) sub_1 (b) sub_2 (c) sub_3

(d) sub_4 (e) sub_5 (f) sub_6

Figure 11: Abstracted map combinations.

Table 1: Statistical information of the maps.

| | sub_1 | sub_2 | sub_3 | sub_4 | sub_5 | sub_6 | original map |
|---|---|---|---|---|---|---|---|
| period/min | 0-255 | 256-375 | 376-595 | 596-980 | 981-1160 | 1161-1440 | 0-1440 |
| Duration/min | 255 | 120 | 220 | 385 | 180 | 280 | 1440 |
| Node.Num | 855 | 967 | 1291 | 1103 | 1236 | 970 | 2573 |
| Link.Num | 1675 | 1877 | 2715 | 2205 | 2608 | 1883 | 6724 |
| Avg.dense/(veh/mile/lane) | 0.025 | 0.598 | 3.848 | 2.102 | 3.107 | 0.566 | 1.702 |
| Std.dense | 0.016 | 0.451 | 1.110 | 0.097 | 0.550 | 0.436 | 1.458 |

(Note: Avg.dense = Average density, Std.dense = standard deviation of density).

The prediction performance of the abstracted map scenario is close to that of the full static map scenario. The errors of the predicted traffic pattern, which are described by the average travel time and the average travel distance, are both less than 5%. In Jafari's contraction simulation experiment [15], the vehicle travel time error between the complete network and contracted network is reported to be less than 6.7%. Taking Jafari's work as a benchmark, we conclude that the proposed method can ensure analysis accuracy.

Meanwhile, among the total 529,336 vehicles, 194,121 were affected by the map abstraction. The error of the affected vehicles' average travel times between two maps was 0.15 minute, and the difference ratio was less than 3%. The impact of boundary issues is therefore manageable, as the travel time error is small compared with the full static map.

On the other hand, the CPU time savings were roughly 25%, which proves that the abstracted map can alleviate computational burden to a great extent. Furthermore, the comparison of the CPU time with the sketch map validates that the map with the lowest fidelity may contradictorily produce the worst efficiency. The substantial growth of the vehicle average travel time confirms that the excessive deletion of links, especially critical links, leads to additional congestion and takes extra computational time.

Figure 12 further presents the CPU times of simulation and assignment components over iterations in SBDTA. The performance of the three maps was compared. These were the original detailed map, the abstracted dynamic map, and the sketch map. One can tell that the abstracted dynamic map takes less computational time than the original detailed map, in both simulation and assignment. This is because the abstracted dynamic map omits overwhelming operations on noncritical links in the simulation process and omits reaching for noncritical links in the time-dependent shortest path (TDSP) portion of the assignment process.

It can also be found that the sketch map takes more CPU time in simulation and assignment than both the abstracted dynamic map and the original detailed map. The extension of simulation CPU time is closely related to the additional vehicles caused by congestion. The impact of massive link reduction on assignment can be summarized in two aspects. On one hand, fewer links need to be calculated

Table 2: Experiment validation results.

| | Avg.time/min | Avg.dist/mile | Aff.time/min | CPU/sec |
|---|---|---|---|---|
| Abstracted map | 5.869 | 5.044 | 5.857 | 10389.38 |
| Original map | 5.607 | 4.818 | 6.010 | 13833.80 |
| Sketch map | 11.641 | 5.533 | — | 11664.33 |
| Error (%) | 4.67 | 4.69 | 2.55 | — |
| En.eff(%) | — | — | — | 24.90 |

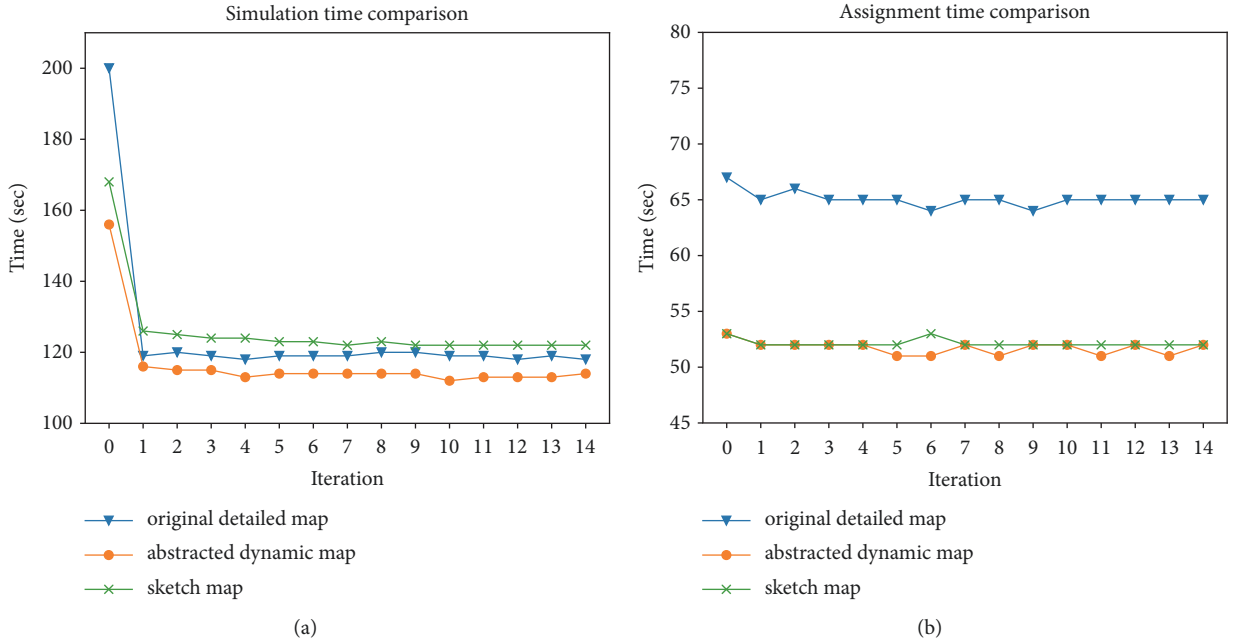


Figure 12: CPU times of simulation and assignment over iterations in SBDTA. A comparison between the original detailed map scenario, abstracted dynamic map scenario, and sketch map scenario.

in TDSP, which saves computational time in the spatial dimension. On the other hand, the congestion caused by the sketch map leads to longer search times in TDSP for the same OD pair. The interplay of the computational time reduction in the spatial dimension and the corresponding increment in the temporal dimension eventually reaches a balance condition, resulting in almost identical assignment computational times.

Figure 13 shows the Cumulative Distribution Function (CDF) of travel time frequency in original detailed map and abstracted dynamic map. It can be observed that the two function curves are close to each other, with the abstracted dynamic map having a slightly higher frequency at the tail end. A Student's t-test is performed with a significance level of 0.05. As the P-value is equal to 0.999, we fail to reject the null hypothesis, meaning that there exists no significant difference between the average travel times of the two maps, and that the abstracted dynamic map maintains a similar performance compared to the original detailed map.

The relative gap for the DUE condition is usually adopted as the convergence criterion of SBDTA. Figure 14 shows the convergence performance of the original detailed map, the abstracted dynamic map and the sketch map, respectively. In the initial iterations, the abstracted dynamic map scenario performs worse than the original detailed map scenario, but it converges more rapidly to a stabilized state. The faster convergence is mainly due to efficient path searching since less route options are available for choosing in the abstracted dynamic map. Less links means less route options, and thus vehicles will converge to the shortest path faster. However, the excessive link deletion and congestion in the sketch map result in an inappropriate step size and increase the convergence iteration step number. After 15 iterations, all scenarios converge with their relative gaps decreasing to close to 0%.

Comparing the accumulation volume of the abstracted dynamic map with the original detailed map, we see the equilibrium flow pattern shown in Figure 15, with (a) and (b) representing the situations of each subinterval and the whole analysis period, respectively. We use a one-dimensional linear equation to fit all samples, and the fitting result is shown in Table 3. With each color representing a subinterval's equilibrium flow pattern, Figure 15(a) reveals that the abstracted dynamic maps with less links removed have network performances more consistent with the original detailed map. Figure 15(b) proves that the overall performance of the

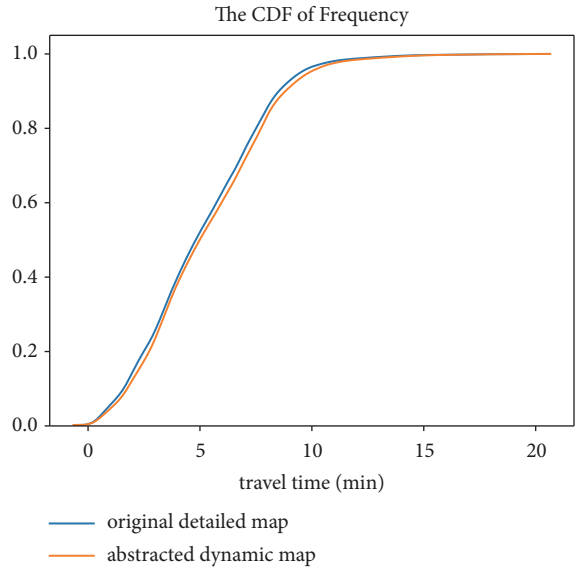


Figure 13: The CDF of travel time frequency in original detailed map and abstracted dynamic map.

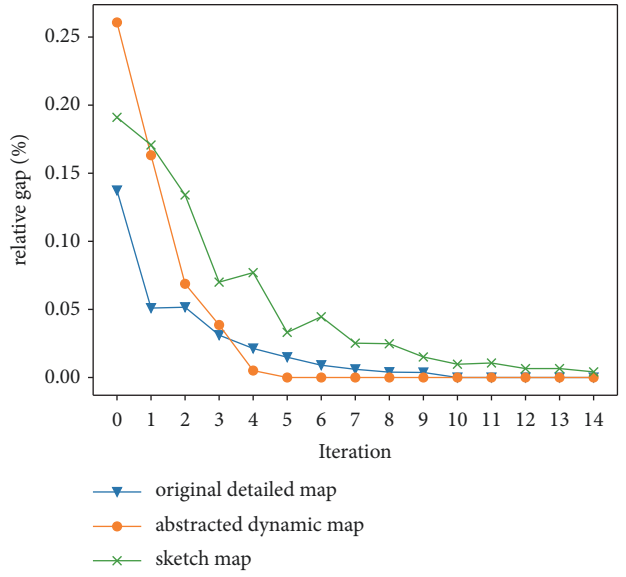


Figure 14: Convergence results.

abstracted dynamic map is basically consistent with that of the original detailed map.

## 4. Conclusions

This paper presented an innovative MFD-based spatiotemporal dynamic map abstraction method that can adaptively segment the planning horizon and carry out abstraction in each subinterval to obtain a proper-fidelity map for traffic analysis. The proposed abstraction method is able to balance the efficiency and accuracy of traffic analysis. The main conclusions are summarized below:

(1) Compared to static maps, the proposed framework of the spatiotemporal dynamic map provides an operable way to adjust fidelity in both spatial and temporal dimensions and is able to capture heterogeneity. The efficiency enhancement and accuracy verify the feasibility of the proposed method.

(2) MFD can be adopted to identify temporal traffic heterogeneity. This paper provides a new application of MFD in the traffic planning field. Additionally, the proposed planning horizon segmentation algorithm ATICC effectively solves the segmentation critical point jumping issue that may exist in conventional clustering methods. ATICC produces subintervals with distinct MFD characteristics.

(3) Taking the traffic dynamics into consideration, CEA realizes a dynamic map abstraction and captures critical links. The boundary issue strategies reasonably respond to the deletion of noncritical links and greatly reduce the

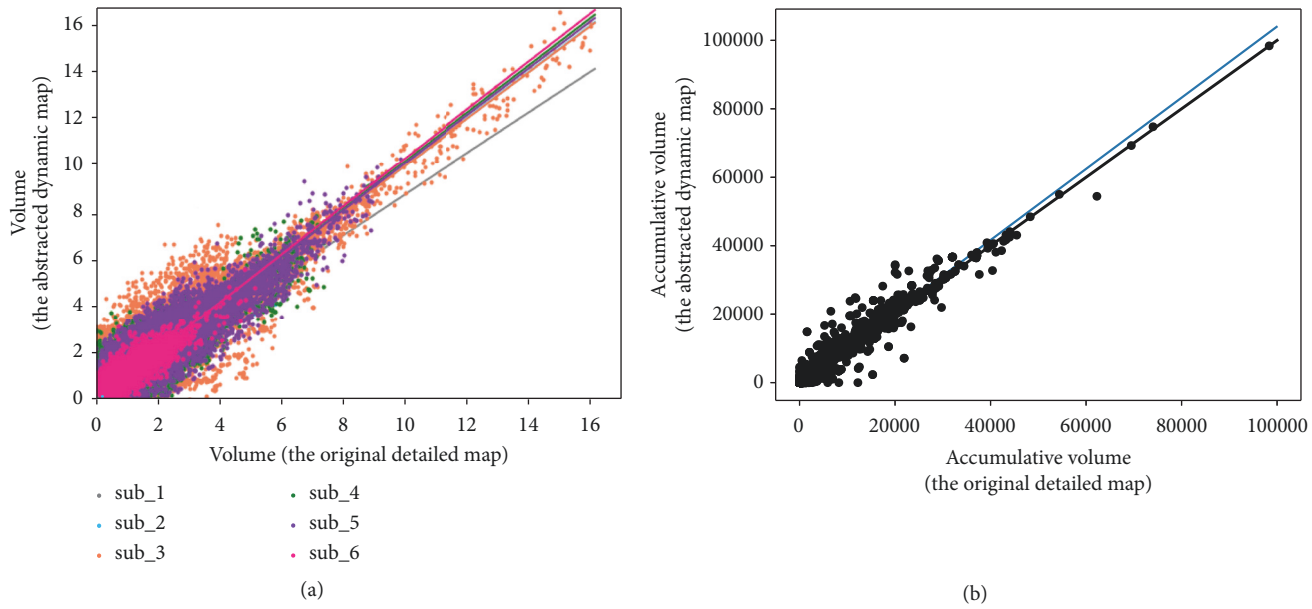


Figure 15: Equilibrium flow pattern.

Table 3: Fitting results.

| | coefficient | R-square |
|---|---|---|
| sub_1 | 0.869 | 0.457 |
| sub_2 | 1.020 | 0.873 |
| sub_3 | 1.013 | 0.927 |
| sub_4 | 1.034 | 0.910 |
| sub_5 | 1.023 | 0.934 |
| sub_6 | 1.058 | 0.859 |
| accu_vol | 1.044 | 0.963 |

computational burden in both simulation and assignment in SBDTA.

The abstraction of an analysis map only needs to be performed once and the resulting abstracted map can be applied to future scenarios. However, the MFD used in our experiment is actually an artificial MFD, which is calculated from a simulation run. It would be more reasonable to use a MFD calculated from detector data, and it remains to be further explored.

## Data Availability

The Alexandria network data used to support the findings of this study are available from the corresponding author upon request.

## Conflicts of Interest

The authors declare that there is no conflict of interest regarding the publication of this paper.

## Acknowledgments

This research was sponsored by the National Key Research and Development Plan of China (2018YFB1600800), the Shanghai "Sailing" talent program (19YF1451200), the Shanghai Science and Technology Committee project (19692108700), and Fundamental Research Funds for the Central Universities (22120180622).

## References

[1] J. Barceló, *Fundamentals of traffic simulation*, vol. 145, Springer, 2010.

[2] V. A. Vu and G. Tan, "High-performance mesoscopic traffic simulation with GPU for large scale networks," in *Proceedings of the 21st IEEE/ACM International Symposium on Distributed Simulation and Real Time Applications, DS-RT 2017*, pp. 1–9, IEEE Press, Italy, October 2017.

[3] Y.-C. Chiu et al., Dynamic traffic assignment: A primer. Transportation Research Circular, 2011(E-C153).

[4] S. Peeta and A. K. Ziliaskopoulos, "Foundations of dynamic traffic assignment: The past, the present and the future," *Networks And Spatial Economics*, vol. 1, no. 3-4, pp. 233–265, 2001.

[5] Y. Tian, Y. Chiu, and J. Sun, "Understanding behavioral effects of tradable mobility credit scheme: An experimental economics approach," *Transport Policy*, vol. 81, pp. 1–11, 2019.

[6] R. R. Barton and D. W. Hearn, *Network aggregation in transportation planning models*, United States. Dept. of Transportation. Research and Special Programs, 1979.

[7] A. E. Haghani and M. S. Daskin, "Network design application of an extraction algorithm for network aggregation," *Transportation Research Record*, vol. 944, pp. 37–46, 1983.

[8] C. Wei and P. M. Schonfeld, "An artificial neural network approach for evaluating transportation network improvements," *Journal of Advanced Transportation*, vol. 27, no. 2, pp. 129–151, 1993.

[9] J. Chen, Y. Hu, Z. Li, R. Zhao, and L. Meng, "Selective omission of road features based on mesh density for automatic map generalization," *International Journal of Geographical Information Science*, vol. 23, no. 8, pp. 1013–1032, 2009.

[10] I. D. Wilson, J. Ware, and J. Ware, "A Genetic Algorithm approach to cartographic map generalisation," *Computers in Industry*, vol. 52, no. 3, pp. 291–304, 2003.

[11] J. Renard and S. Rousic, A Practical Experience on Road Network Generalisation for Production Device.

[12] W. Smith, "The effect of zone size on traffic assignment and trip distribution," *Commonwealth Bureau of Roads*, 1971.

[13] R. Eash et al., "Equilibrium traffic assignment on an aggregated highway network for sketch planning," *Transportation Research*, vol. 13, pp. 243–257, 1979.

[14] S. D. Boyles, "Bush-based sensitivity analysis for approximating subnetwork diversion," *Transportation Research Part B: Methodological*, vol. 46, no. 1, pp. 139–155, 2012.

[15] E. Jafari and S. D. Boyles, "Improved bush-based methods for network contraction," *Transportation Research Part B: Methodological*, vol. 83, pp. 298–313, 2016.

[16] L. Zhu and Y.-C. Chiu, "Transportation routing map abstraction approach: Algorithm and numerical analysis," *Transportation Research Record*, vol. 2528, pp. 78–85, 2015.

[17] L. Zhu, Y. Chiu, and Y. Chen, "Road network abstraction approach for traffic analysis: framework and numerical analysis," *IET Intelligent Transport Systems*, vol. 11, no. 7, pp. 424–430, 2017.

[18] J. Shelton et al., *Comparative Software Analysis of Regional Binational Modeling*, 2016, Comparative Software Analysis of Regional Binational Modeling.

[19] B. Greenshields, W. Channing, and H. Miller, "A study of traffic capacity," in *Highway Research Board Proceedings*, National Research Council (USA), Highway Research Board, 1935.

[20] N. Geroliminis and C. F. Daganzo, "Existence of urban-scale macroscopic fundamental diagrams: some experimental findings," *Transportation Research Part B: Methodological*, vol. 42, no. 9, pp. 759–770, 2008.

[21] N. Geroliminis and C. F. Daganzo, "Macroscopic modeling of traffic in cities," in *Proceedings of the Transportation Research Board 86th Annual Meeting*, No. 07-0413 pages.

[22] C. F. Daganzo and N. Geroliminis, "An analytical approximation for the macroscopic fundamental diagram of urban traffic," *Transportation Research Part B: Methodological*, vol. 42, no. 9, pp. 771–781, 2008.

[23] N. Geroliminis and J. Sun, "Properties of a well-defined macroscopic fundamental diagram for urban traffic," *Transportation Research Part B: Methodological*, vol. 45, no. 3, pp. 605–617, 2011.

[24] K. An, Y. Chiu, X. Hu, and X. Chen, "A network partitioning algorithmic approach for macroscopic fundamental diagram-based hierarchical traffic network management," *IEEE Transactions on Intelligent Transportation Systems*, vol. 99, pp. 1–10, 2017.

[25] Z. Zhou, S. Lin, and Y. Xi, "A fast network partition method for large-scale urban traffic networks," *Control Theory and Technology*, vol. 11, no. 3, pp. 359–366, 2013.

[26] V. L. Knoop, S. P. Hoogendoorn, and J. W. C. van Lint, "Routing strategies based on macroscopic fundamental diagram," *Transportation Research Record*, vol. 2315, pp. 1–10, 2012.

[27] T. Yoshii, Y. Yonezawa, and R. Kitamura, "Evaluation of an area metering control method using the macroscopic fundamental diagram," in *Proceedings of the in World Conference on Transport Research*, 2010.

[28] M. D. Simoni, A. J. Pel, R. A. Waraich, and S. P. Hoogendoorn, "Marginal cost congestion pricing based on the network fundamental diagram," *Transportation Research Part C: Emerging Technologies*, vol. 56, pp. 221–238, 2015.

[29] N. Zheng and N. Geroliminis, "Modeling and optimization of multimodal urban networks with limited parking and dynamic pricing," *Transportation Research Part B: Methodological*, vol. 83, pp. 36–58, 2016.

[30] A. Pascale, D. Mavroeidis, and H. T. Lam, "Spatiotemporal clustering of urban networks: Real case scenario in London," *Transportation Research Record*, vol. 2491, pp. 81–89, 2015.

[31] K. Ampountolas, N. Zheng, and N. Geroliminis, "Macroscopic modelling and robust control of bi-modal multi-region urban road networks," *Transportation Research Part B: Methodological*, vol. 104, pp. 616–637, 2017.

[32] S. Kim, S. Tak, and H. Yeo, "Agent-based network transmission model using the properties of macroscopic fundamental diagram," *Transportation Research Part C: Emerging Technologies*, vol. 93, pp. 79–101, 2018.

[33] S. Kim and H. Yeo, "Evaluating link criticality of road network based on the concept of macroscopic fundamental diagram," *Transportmetrica A: Transport Science*, vol. 13, no. 2, pp. 162–193, 2016.

[34] Y. Tian and Y.-C. Chiu, "Numerical analysis for adaptive traffic simulation," *Transportation Research Record*, no. 2316, pp. 132–139, 2012.

[35] D. Hallac, S. Vare, S. Boyd, and J. Leskovec, "Toeplitz inverse covariance-based clustering of multivariate time series data," in *Proceedings of the 23rd ACM SIGKDD International Conference on Knowledge Discovery and Data Mining, KDD 2017*, pp. 215–223, Canada, August 2017.

[36] J. Friedman, T. Hastie, and R. Tibshirani, "Sparse inverse covariance estimation with the graphical lasso," *Biostatistics*, vol. 9, no. 3, pp. 432–441, 2008.

[37] R. L. Graham and P. Hell, "On the history of the minimum spanning tree problem," *Annals of the History of Computing*, vol. 7, no. 1, pp. 43–57, 1985.

[38] G. B. Dantzig, "On the Shortest Route Through a Network," *Management Science*, vol. 6, no. 2, pp. 187–190, 1960.

[39] Y.-C. Chiu et al., *Dynust User's Manual*, University of Arizona, Tucson, 2011.

[40] Y. Tian and Y.-C. Chiu, "A variable time-discretization strategies-based, time-dependent shortest path algorithm for dynamic traffic assignment," *Journal of Intelligent Transportation Systems: Technology, Planning, and Operations*, vol. 18, no. 4, pp. 339–351, 2014.

[41] M. Haklay, "How Good is Volunteered Geographical Information? A Comparative Study of OpenStreetMap and Ordnance Survey Datasets," *Environment and Planning B: Planning and Design*, vol. 37, no. 4, pp. 682–703, 2010.